Research Square

Preprints are preliminary reports that have not undergone peer review.
They should not be considered conclusive, used to inform clinical practice,
or referenced by the media as validated information.

Age-related choroid plexus cystic remodeling: A study of healthy individuals based on high-resolution MRI

Zhiming Zhen
Army Medical University
Suyi Zhou
Army Medical University
Liuqi Yang
Sichuan Science City Hospital
Zhe Sun
Second Affiliated Hospital of Zhejiang University
Miao Lin
Second Affiliated Hospital of Zhejiang University
Yanqiu Hua
Army Medical University
Dandan Yuan
Army Medical University
Yi-Cheng Hsu
Siemens (China)
Zhentao Zuo
University of Chinese Academy of Sciences
Peiyu Huang
Second Affiliated Hospital of Zhejiang University
Chen Liu
Army Medical University
Wei Chen
landcw@tmmu.edu.cn

Army Medical University

Research Article

Keywords: choroid plexus, choroid plexus cyst, aging, magnetic resonance imaging, high-resolution MRI

Posted Date: November 10th, 2026

DOI: https://doi.org/10.21203/rs.3.rs-11334747/v1

License: This work is licensed under a Creative Commons Attribution 4.0 International License.
Read Full License

Additional Declarations: No competing interests reported.

Abstract

Background

The choroid plexus (CP) plays a critical role in maintaining brain homeostasis. Choroid plexus cysts (CPCs) have traditionally been regarded as uncommon incidental findings but have recently gained attention as potential imaging markers of aging and neurodegeneration. This study aimed to systematically characterize the prevalence, morphometric features, and age-related patterns of CPCs in healthy adults using high-resolution MRI.

Methods

In this cross-sectional observational study, 132 healthy volunteers (76 younger adults aged 20–40 years and 56 older adults aged 41–80 years) underwent three-dimensional heavily T2-weighted MRI. CPCs were identified and classified into two imaging phenotypes, cerebrospinal fluid (CSF)-like and hypointense, according to their T2 signal characteristics. Quantitative measures included CPC count, largest CPC volume, and normalized CP volume (CPV). Partial correlation analyses were performed to assess associations among age, CPC measures, and CPV.

Results

CPCs were detected in 59.2% of younger adults and 89.3% of older adults, substantially higher than prevalence reported in previous studies. Older adults had significantly greater CPC counts and larger CPC volumes, and the hypointense phenotype was more prevalent in this group. Age was positively associated with CPC count, largest CPC volume, and CPV. In younger adults, CPV, CPC count, and largest CPC volume were significantly correlated, whereas these relationships became less coupled in older adults. No significant associations were observed between CPC measures and cognitive or sleep scores.

Conclusions

High-resolution MRI reveals that CPCs are common findings even in healthy young adults and become more prevalent and extensive with advancing age. The age-related changes in CPC burden and imaging phenotype suggest that CPC characteristics may provide candidate imaging markers of structural CP remodeling during brain aging.

1. Introduction

The choroid plexus (CP) is a key component of the blood–cerebrospinal fluid barrier (BCSFB) and an important interface between the peripheral circulation and the central nervous system[1]. Beyond its

well-established role in cerebrospinal fluid (CSF) production, the CP is involved in solute transport, immune surveillance, waste clearance, and the maintenance of brain homeostasis [2]. Growing evidence has implicated CP dysfunction in a wide range of neurological disorders [3]. However, its deep anatomical location and intricate morphology have posed persistent challenges for in vivo investigation. highlighting the importance of characterizing CP structure and function in vivo to better understand disease mechanisms and facilitate the development of CP-targeted therapeutic strategies [4].

MRI-derived measures of the CP, particularly CP volume (CPV), have increasingly been investigated as potential imaging biomarkers [5]. In cerebral small vessel disease, enlarged CPV has been associated with white matter hyperintensity progression, potentially reflecting disturbances in CSF dynamics [6]. In Alzheimer's disease (AD), CP enlargement has been linked to impaired amyloid-β (Aβ) clearance and accelerated cognitive decline; this association potentially reflect CP-related secretory dysfunction, as CP-derived extracellular vesicles have been shown to modulate hippocampal function [7]. CP enlargement has also been reported in individuals with long COVID and cognitive impairment [8]. Collectively, these findings suggest that CPV may serve as a nonspecific marker of CP involvement across diverse disease conditions. However, volumetric measures alone provide only a coarse characterization of CP remodeling. A more detailed assessment of CP morphology and age-related structural alterations is therefore needed to better distinguish physiological variation from disease-related changes.

More recently, choroid plexus cysts (CPCs) have emerged as a potentially informative morphological feature of aging and neurodegeneration. A greater CPC burden has been reported in older than in younger adults[9], while another study using high-resolution 3T FLAIR imaging identified a higher CPC burden in amyloid-positive individuals with cognitive impairment[10]. In our previous work using 7T MRI to visualize the fine structural features of the CP, we observed a high prevalence of CPCs in patients with neurodegenerative disorders, frequently appearing as clustered cystic structures with a characteristic "grape-like" configuration [11]. These observations suggest that cystic changes may represent an important component of CP structural remodeling. Notably, however, the reported prevalence of CPCs varies markedly across studies, ranging from approximately 8.2%–16.3% in populations aged 60–90 years to > 80% in cohorts with mean ages of 71–79 years, and from approximately 30% to 95% in cohorts aged 56–69 years[12]. Such substantial variability suggests that CPC detection is strongly influenced by MRI spatial resolution, sequence contrast, and imaging protocol. Consequently, many small or subtle CPCs may have remained undetected in previous studies, and their true prevalence and physiological significance remain incompletely understood.

In the present study, we optimized the visualization of CPCs using high-resolution three-dimensional (3D) heavily T2-weighted MRI at both 3T and 7T. With these optimized imaging protocols, CPCs were readily visualized even in young adults, revealing a substantially higher prevalence than previously appreciated. We therefore systematically characterized CPC features, including their prevalence, number, volume, and signal-intensity characteristics, and compared these features between young and older adults. By defining the imaging phenotype of CPCs across adulthood, we aimed to determine whether CPCs

represent a common component of physiological CP heterogeneity and to explore how their characteristics may evolve toward age-related structural remodeling.

2. Materials and Methods

2.1 Study Design and Participant Selection

This cross-sectional, observational study was conducted at the First Affiliated Hospital of Army Medical University between June 2025 and January 2026 and comprised two phases. In the first phase, 16 healthy volunteers underwent both 3T and 7T MRI to compare CPC visualization across different magnetic field strengths and to assess the consistency of CPC identification between the two imaging platforms. In the second phase, a larger cohort was recruited for quantitative morphometric analysis. Participants were divided into a younger cohort (YC; *n* = 76; age range, 20–40 years), who underwent 7T MRI, and an older cohort (OC; *n* = 56; age range, 41–80 years), who underwent 3T MRI.

The inclusion criteria were: (1) no history of neurological or psychiatric disorders; and (2) preserved cognitive function, as assessed using the Mini-Mental State Examination (MMSE), with no clinical evidence of cognitive impairment affecting functional independence. Exclusion criteria were: (1) visible intracranial abnormalities on MRI, including brain tumors, large territorial infarctions, or intracranial hemorrhage; (2) a history of intracranial surgery or significant head trauma; (3) systemic diseases that could substantially affect brain structure, such as severe uncontrolled hypertension or diabetes mellitus; and (4) standard contraindications to MRI.

The study was approved by the Ethics Committee of the First Affiliated Hospital of Army Medical University (Approval No. KY2026209). Written informed consent was obtained from all participants before study participation.

2.2 Clinical Assessments

All participants underwent standardized clinical evaluations conducted by trained neuropsychologists. Cognitive function was screened using the MMSE to ensure participants met the criteria for healthy aging. Additionally, subjective sleep quality and patterns were evaluated via the Pittsburgh Sleep Quality Index (PSQI). All clinical evaluations were performed on the same day as the MRI scans to ensure the temporal consistency of the neuropsychological and neuroimaging data.

2.3 MRI Acquisition

Participants in the YC underwent ultra-high-field 7T MRI scanning (MAGNETOM Terra, Siemens Healthcare, Erlangen, Germany) using a 32-channel head coil. Participants in the OC were scanned on a 3.0T MRI system (uMR 770, United Imaging Healthcare, Shanghai, China) using a 32-channel head coil. This field strength allocation was designed to ensure image quality, subject tolerability, and data robustness. The 7T protocol provides superior spatial resolution and SNR, which are advantageous for detecting fine CP microstructural details. However, the 7T imaging was less well tolerated by older

participants. Therefore, 3T MRI was used for the older cohort because it is more widely established in clinical practice, offers better scan tolerability, and is more suitable for individuals who may have age-related fragility, or a higher likelihood of MRI safety concerns such as metallic implants.

The detailed acquisition parameters are summarized as follows: (1)7T MRI Protocols for YC. T2-SPACE: Voxel size = 0.45 × 0.45 × 0.45 mm^3, TR/TE = 4000/263 ms, bandwidth = 744 Hz/Px; UHR-T2WI-TSE: Voxel size = 0.2 × 0.2 × 1.0 mm^3, averages = 4, TR/TE = 6500/76 ms, bandwidth = 168 Hz/Px; T2-FLAIR: Voxel size = 0.7 × 0.7 × 3.0 mm^3, TR/TE/TI = 9000/96/2600 ms, bandwidth = 313 Hz/Px; T1-MP2RAGE: Voxel size = 0.65 × 0.65 × 0.65 mm^3, TR/TE = 4300/2.27 ms, TI1/TI2 = 1000/3200 ms, bandwidth = 200 Hz/Px. (2)3T MRI Protocol for OC. T2-SPACE: Voxel size = 0.58 × 0.58 × 0.58 mm^3, TR/TE = 1300/282.24 ms, bandwidth = 365 Hz/Px; T2-FLAIR: Voxel size = 0.8 × 0.8 × 0.8 mm^3, TR/TE/TI = 6500/438/1938 ms, bandwidth = 600 Hz/Px; T1-MPRAGE: Voxel size = 0.8×0.8×0.8mm^3, TR/TE = 7.2/3.1 ms, TI = 1000 ms, bandwidth = 275 Hz/Px.

2.4 MRI Postprocessing and Image Analysis

CPC identification and measurement were performed using a standardized imaging protocol. T2-FLAIR and T1-weighted images were first reviewed to characterize CP signal and to exclude other CP abnormalities, such as xanthogranulomas. T2-SPACE images were then used for multiplanar reconstruction and three-dimensional assessment of CPC morphology and size. CPCs were defined as round or oval cystic structures located within the CP and visible on at least two orthogonal planes [11]. Based on the signal intensity of the cystic content on T2-SPACE images, CPCs were classified into two imaging phenotypes: (1) **CSF-like CPCs**, defined as cysts with internal signal intensity similar to that of surrounding CSF; and (2) **hypointense CPCs**, defined as cysts with internal signal intensity lower than that of the surrounding CSF (Fig. 1).

For size assessment, the largest CPC in each hemisphere was identified. A neurologist with expertise in neuroimaging measured its maximum length (L), width (W), and height (H) on multiplanar reconstructed T2-SPACE images. CPC volume was estimated using the ellipsoid formula: V = $\frac{\pi}{6}$ × L × W × H.

For CPC counting, two radiologists (D.Y. and Z.Z., each with 5 years of experience in neuroimaging), independently recorded the total number of CPCs in both hemispheres. Inter-rater reliability for CPC counts was assessed using the intraclass correlation coefficient (ICC) based on a two-way random-effects model. An ICC greater than 0.75 was considered indicative of good agreement. Discrepancies in CPC identification or counting were resolved by consensus after joint review with a senior neuroradiologist with more than 15 years of neuroimaging experience.

2.5 MRI volumetric analysis

Volumetric analysis was performed using FreeSurfer (version 7.2.0; http://surfer.nmr.mgh.harvard.edu) following the standard recon-all processing pipeline. Quantitative measures included total intracranial volume (TIV), cortical gray matter volume, lateral ventricular volume, choroid plexus volume (CPV),

hippocampal volume, and white matter hyperintensity (WMH) volume. All segmentation outputs were visually inspected for anatomical accuracy and manually corrected when necessary by two neuroradiologists (D.Y. and Z.Z.), each with 5 years of neuroimaging experience. To account for interindividual differences in head size, CPV was normalized to TIV and expressed as CPV/TIV × 1000.

Because CPCs were poorly visualized on conventional T1-weighted images (Fig. 1F), their cystic cavities were not included in the FreeSurfer-derived CP segmentation. Accordingly, CPV in the present study primarily represented the solid tissue component of the CP rather than the combined volume of CP tissue and CPCs.

3. Statistical Analysis

Continuous variables are presented as mean ± standard deviation (SD) or median with interquartile range (IQR), as appropriate, according to their distributions assessed using the Shapiro–Wilk test. Categorical variables are presented as frequencies and percentages.

Statistical analyses were performed in two stages. First, in the 16 participants who underwent all three imaging protocols (3T T2-SPACE, 7T T2-SPACE, and 7T 2D-TSE), CPC measurements were compared across sequences using the Friedman test. Cross-sequence agreement for CPC counts between 3T and 7T SPACE in these 16 participants was further quantified using the intraclass correlation coefficient (ICC; two-way random-effects model, absolute agreement, single measurement). When a significant overall difference was identified, pairwise comparisons were performed using Wilcoxon signed-rank tests with Bonferroni correction for multiple comparisons.

Second, for comparisons between the YC and OC, normally distributed continuous variables were compared using independent-samples t tests, whereas non-normally distributed variables were compared using Mann–Whitney U tests. Categorical variables were compared using Pearson's chi-square test or Fisher's exact test, as appropriate.

Partial correlation analyses adjusted for sex were performed to examine the relationships of CPC characteristics, including CPC count and CPC volume, with age, CP volume, and clinical measures, including MMSE and PSQI scores. Pearson partial correlation was used for normally distributed variables, whereas partial Spearman correlation was used for non-normally distributed variables.

All statistical analyses were performed using SPSS Statistics (version 26.0; IBM Corp., Armonk, NY, USA). Data visualization was performed using R (version 4.3.0) and OriginPro (version 2021). All statistical tests were two-sided, and a P value < 0.05 was considered statistically significant.

4. Results

4.1 Visualization of CPCs on 3T and 7T MRI

Regarding CPC visualization across different MRI protocols, 16 volunteers (mean age, 55.0 ± 8.6 years; 43.75% male) underwent 3T T2-SPACE, 7T T2-SPACE, and 7T 2D-TSE imaging. For CPC counting, independent assessments by two radiologists demonstrated good inter-rater reliability, with an ICC of 0.85 (95% CI, 0.76–0.91). The signal intensity characteristics of CPCs, including CSF-like and hypointense phenotypes, were consistently observed across both 3T and 7T SPACE images.

The number of detected CPCs did not differ significantly between the 7T SPACE and 3T SPACE sequences [11.0 (8.0–15.0) vs. 10.0 (7.0–13.0), $P > 0.05$; Fig. 2]. In contrast, the 7T 2D-TSE sequence detected significantly fewer CPCs [7.0 (5.0–9.0)] than both SPACE sequences (both $P < 0.05$). Across the 16 volunteers, CPC counts showed excellent cross-protocol agreement between 3T SPACE and 7T SPACE (ICC (2,1) = 0.92; 95% CI, 0.74–0.97)

4.2 Demographic Characteristics and Age-Related Differences in CPC Prevalence and Phenotypes

A total of 132 healthy volunteers were included, comprising 76 younger adults and 56 older adults. As summarized in Table 1, sex distribution did not differ between the younger cohort (YC) and the older cohort (OC) ($\chi^2 = 0.002$, $P = 0.964$). Compared with the YC, the OC had significantly lower MMSE scores ($Z = 3.70$, $P < 0.001$) and higher PSQI scores ($Z = -3.34$, $P = 0.001$), indicating relatively lower cognitive performance and poorer subjective sleep quality, respectively.

CPC prevalence differed significantly between the two age groups, with CPCs identified in 50 of 56 participants (89.3%) in the OC compared with 45 of 76 participants (59.2%) in the YC ($\chi^2 = 14.46$, $P < 0.001$, Table 1, Fig. 3). Among participants with CPCs, the distribution of CPC imaging phenotypes also differed between groups. Hypointense CPCs were more frequently observed in the OC than in the YC, whereas CSF-like CPCs were more common in the YC ($\chi^2 = 7.17$, $P < 0.01$). Representative CPC phenotypes and the appearance of the CP in participants without visible CPCs are shown in Fig. 4. No significant sex difference in CPC prevalence was observed within either age cohort (both $P > 0.05$, Fisher's exact test).

Table 1
Baseline Demographic and Clinical Data for the Participant Groups

Age, years *	**Young cohort (*n* = 76)**	**Older cohort (*n* = 56)**	***t*/χ^2/*Z***	***P* value**
	23.93 ± 4.08	**61.16 ± 11.46**	**-**	**-**
Sex, male, n (%)	22 (28.94)	16 (28.57)	0.002	0.964
MMSE score	30.0 (29.0,30.0)	29.0(26.0,30)	3.70	< 0.001***
PSQI score	5.0 (2.5,6.5)	9.0 (5.0,17.0)	-3.342	0.001**
R_CPCs number†	6.0 (3.3,7.0)	7.0 (5.0,10.3)	-3.653	< 0.001***
L_CPCs number†	6.0 (3.0,8.0)	7.0 (5.8,10.3)	-2.516	0.012*
R_CPCs volume, mm^3†	12.5 (6.1,34.6)	33.5 (12.3,73.1)	-2.128	0.033*
L_CPCs volume, mm^3†	9.4 (4.3,36.3)	36.4 (10.9,67.0)	-3.151	0.002**
Total CPC count†	12.0 (8.0,14.8)	15.0 (10.0,21.0)	-3.465	0.001**
Largest CPCs volume, mm^3†	26.9 (12.7,70.5)	72.9 (31.3,137.9)	-2.917	0.004**
CPC signal phenotype† (CSF-like /hypointense)	36/9	27/23	7.170	< 0.01**
CPV/TIV × 10^3	0.73 (0.5,0.9)	1.04 (0.9,1.3)	-3.443	0.001**

Notes: Data are presented as mean ± standard deviation, median (interquartile range), or number (percentage), as appropriate. MMSE, Mini-Mental State Examination; PSQI, Pittsburgh Sleep Quality Index; CPC, choroid plexus cyst.

* Age was used to define the study groups and was therefore not subjected to statistical comparison. † Statistical comparisons were performed only among participants with CPCs.

(A) Overall prevalence of CPCs in the younger cohort (YC) and older cohort (OC). Green and light-green segments indicate participants with and without CPCs, respectively. (B) Distribution of CSF-like and hypointense CPC phenotypes in the YC and OC. (C, D) Sex-based comparisons of CPC prevalence within the YC and OC, respectively. Orange and blue segments indicate participants with and without CPCs, respectively. Statistical comparisons were performed using Fisher's exact test where applicable (***P < 0.001). Sample sizes (n) are shown in parentheses.

4.3 CPC burden and CP volume

Among participants with detectable CPCs, the OC showed a greater CPC burden and larger normalized CPV than the younger cohort YC. The total number of CPCs was higher in the OC than in the YC (15.00 [10.00–21.00] vs. 12.00 [8.00–14.80], P = 0.001). Similarly, the bilateral largest-CPC volume was significantly greater in the OC (72.98 [31.3–137.9] vs. 26.95 [12.7–70.5], Z = − 2.917, P = 0.004).

Normalized CPV was significantly greater in the OC than in the YC (1.045 [0.9–1.3] vs. 0.732 [0.5–0.9], $P = 0.001$).

Collectively, these findings indicate that older age is associated with greater CPC number and size, together with a larger solid-tissue component of the CP.

(A, B) Representative images from an older participant showing coexisting hypointense CPCs (orange arrowheads) and CSF-like CPCs (green arrowheads). (C, D) Representative images from a younger participant showing exclusively CSF-like CPCs (green arrowheads). (E, F) Representative images from a younger participant without visible CPCs, demonstrating the typical appearance of the choroid plexus within the lateral ventricles.

4.4 Associations of CP and CPC characteristics with age and clinical measures

Age was significantly and positively associated with all assessed CP morphometric measures (Fig. 5). Specifically, age correlated with total CPC count ($r = 0.44$, $P < 0.001$), largest-CPC volume ($r = 0.40$, $P < 0.001$), the number of hypointense CPCs ($r = 0.40$, $P = 0.019$), and normalized CPV ($r = 0.61$, $P < 0.001$).

In the overall population, normalized CPV was positively correlated with both total CPC count ($r = 0.40$, $P < 0.001$, Fig. 6) and bilateral largest-CPC volume ($r = 0.33$, $P < 0.001$). In the YC, normalized CPV significantly associated with bilateral largest-CPC volume ($r = 0.25$, $P = 0.03$). In contrast, no significant associations were observed in the OC between normalized CPV and either total CPC count or largest-CPC volume.

No significant correlations were observed between CP-related morphometric measures, including normalized CPV, total CPC count, and largest-CPC volume, and clinical measures of cognitive function or sleep quality, as assessed by the MMSE and PSQI, respectively (all $P > 0.05$).

In addition, no significant differences in regional gray matter or white matter volumes or clinical scores were observed between CPC-positive and CPC-negative participants in the YC, or between participants with and without hypointense CPCs in the OC (all $P > 0.05$).

5. Discussion

In this study, we demonstrate that CPCs are not rare incidental findings, but may represent a widespread structural feature of the aging CP. Our primary findings are as follows: (1) CPCs were detected in 59.2% of the YC, indicating that a substantial cystic component of the CP may have been under-recognized using conventional MRI protocols. (2) CPC prevalence increased markedly with age, reaching 89.3% in older adults, and was accompanied by a significantly greater bilateral largest-CPC volume, suggesting that CPCs may serve as imaging markers of cerebral aging. (3) We identified two distinct cystic signal phenotypes: a CSF-like phenotype and a hypointense phenotype. The hypointense phenotype was

significantly more frequent in older adults, potentially reflecting age-related changes in intracystic content.

Although our earlier 7T 2D T2-TSE sequences offered exceptional in-plane resolution (0.2 × 0.2 mm), their limited through-plane coverage restricted comprehensive evaluation of CPC spatial architecture[11]. CPCs may depend partly on CSF–blood hydrostatic pressure gradients to maintain their cystic configuration. As a result, they may collapse under ex vivo conditions, which could explain why they are difficult to consistently identify in animal models or postmortem specimens[13, 14]. The 3D heavily T2-weighted sequences at both 3T and 7T used in this study support multiplanar reconstruction, enabling high-fidelity visualization of thin-walled structures and thereby offering a more practical and robust framework for anatomical characterization and quantification of CPCs (Fig. 2). While 3T imaging does not match the clarity of 7T, the absence of significant differences in CPC counting and dominant cyst measurements between the two platforms supports the wider applicability of the "grape sign" across different field strengths. Hypointense CPCs were readily identifiable on the SPACE sequence but were poorly visualized on the TSE sequence. The hypointense appearance likely reflects T2 shortening resulting from proteinaceous material or paramagnetic mineral deposits—a contrast mechanism that is more effectively exploited by the effective TE and heavily T2-weighted nature of the SPACE sequence.

One of the most important findings of this study is the high detection rate of CPCs in healthy younger adults. The 59.2% prevalence observed in the YC is substantially higher than previously reported in neuroimaging studies. For example, an analysis based on the Human Connectome Project Aging dataset reported a much lower prevalence of approximately 4.6% in younger individuals[12]. Fetal choroid plexus cysts are detected by ultrasound in 0.5–2.5% of pregnancies, with more than 90% of isolated cases showing spontaneous resolution before term[15]. This striking discrepancy between the low fetal detection rate and the high prevalence observed in our young adult cohort raises the possibility that many CPCs may not truly "resolve" during development. We suggest that this discrepancy is likely attributable, at least in part, to differences in spatial resolution and sequence sensitivity rather than solely to sampling variation. Our data suggest that CPCs represent a widespread anatomical phenomenon in healthy, cognitively normal young adults. Given the absence of significant differences in cerebral architecture or neuropsychological scores between CPCs-positive and CPC-negative individuals in the YC. It appears that these microcysts do not directly impair cognitive function during early adulthood. Although the definitive boundary between "physiological" and "pathological" cysts remains to be established, these findings demonstrate that CPCs alterations are no longer incidental occurrences.

The OC exhibited a more pronounced cyst burden compared to the YC, with hypointense CPCs being more prevalent within the OC. These findings suggest that CPCs may represent a degenerative marker that continues to evolve with advancing age. Previous research in cognitively intact, Aβ/tau-negative elderly populations (mean age 71.09 ± 7.07) reported a CPCs prevalence of 88.4% (229/259) using 3T 3D-FLAIR (1 mm^3 isotropic resolution) [10]. In the present study, the application of higher-resolution 3T imaging with 0.58-mm isotropic resolution further supports the high prevalence of CPCs during senescence. From a pathophysiological standpoint, the CP is among the brain's most vascularized tissue

and undergoes pronounced capillary basement membrane thickening and pathological interstitial collagen deposition during aging. This is compounded by impaired epithelial transport and clearance functions, including reduced expression or activity of clearance-related proteins, such as the Aβ transporter LRP1[7]. Furthermore, attenuated CP perfusion may contribute to stromal hypoxia, necrosis, and fluid sequestration, fostering a microenvironment that favors cystic remodeling[16]. Age-related increases in BCSFB permeability may further alter the intra-cystic milieu, potentially allowing proteinaceous material, iron-related products, or mineral deposits to accumulate within the cyst cavity[17]. These changes may partly explain the greater frequency of hypointense CPCs in older adults. On the other hand, CPC formation may in turn affect epithelial integrity, ciliary activity, and intraventricular hydrodynamics, thereby leading to altered cerebrospinal fluid turnover and reduced waste clearance capacity, and exacerbating brain degenerative changes [18]. In summary, the pronounced age effect of CPCs supports their potential as a novel neuroimaging biomarker for assessing biological brain age and neurodegenerative risk.

Consistent with previous studies[9], we observed that CPV expands with advancing age, and showed profound positive correlations with both number of CPCs and largest CPCs volume. Although Neuroimaging studies have reported CPV enlargement in aging and neurological disorders, CPCs are usually not captured by T1-weighted volumetric analyses, because of their extremely thin walls and CSF-like T1 signal intensity (Fig. 1F). Thus CPCs are not considered a component of CPV. Enlargement of the CPV and the formation of CPCs may represent distinct dimensions of CP remodeling. CPV enlargement likely reflects pathological alterations in the stroma, vasculature, or epithelium of the solid component [19], whereas CPCs may indicate cystic or fluid-filled cavity remodeling. These two imaging phenotypes are likely to arise from shared underlying biological processes, including chronic inflammation, vascular degeneration, impaired CSF homeostasis, and BCSFB dysfunction [20], without necessarily being causally dependent on each other. Stratified analysis further revealed significant correlations between CPV and both CPC number and bilateral dominant CPC volume within the YC. This finding suggests that, in early adulthood, CP tissue expansion and cystic remodeling may occur in parallel, possibly reflecting a shared structural response to local vascular, stromal, or inflammatory influences. However, this correlation was no longer evident in the OC. One possible explanation is the ceiling effect: Once CPV and CPCs reach their respective physical and physiological capacity thresholds, their growth transitions into a plateau phase, decoupling from the linear escalation of underlying injury [21]. This observation underscores that, in older adults, purely structural indices may become less sensitive to ongoing biological dysfunction. Functional imaging measures, such as CP perfusion, permeability, CSF flow, or molecular imaging markers, may therefore be needed to more comprehensively assess CP physiological integrity in aging populations[22].

Several limitations should be acknowledged. First, as the recruited participants were exclusively cognitively intact healthy volunteers with neuropsychological scores within normative ranges, no significant statistical correlations were identified between CP imaging metrics and clinical scales. Second, while the cross-sectional design effectively illustrates aging trajectories through cohort comparison, longitudinal surveillance is essential to precisely delineate the individual-level transition

from physiological heterogeneity to the pathological "ceiling" of cyst evolution. Third, although the "Grape-sign" may represent the functional attrition of the BCSFB, large-scale investigations are required to establish whether specific cyst-load thresholds or co-occurring inflammatory signatures can definitively validate CPCs as pathological biomarkers. Finally, the younger and older cohorts were scanned at different field strengths (7T vs. 3T). While this may introduce bias, cross-sequence validation in 16 volunteers showed comparable CPC detection between the two systems. Moreover, the older cohort already exhibited significantly greater CPC burden at 3T; 7T would likely have amplified the difference. Thus, our primary conclusions are unlikely to be materially affected by this technical disparity.

In summary, this study uses high-resolution MRI to provide, to our knowledge, the first systematic report of the high prevalence and age-related trajectory of CPC changes in healthy adults, and delineates distinct cystic subtypes. This finding offers a novel imaging framework for understanding age-related remodeling of the BCSFB and the structural underpinnings of brain aging.

Declarations

Ethics approval and consent to participate

The study was approved by the Ethics Committee of Southwest Hospital (First Affiliated Hospital of Army Medical University) (Approval No. KY2026209). All procedures performed in studies involving human participants were in accordance with the ethical standards of the institutional research committee and with the 1964 Declaration of Helsinki and its later amendments. Written informed consent was obtained from all participants before any protocol-specific procedures were performed.

Consent for publication

All authors have approved the manuscript submission. The content of this manuscript has not been published or submitted for publication elsewhere.

Competing interests

The authors declare no competing interests.

Funding

This work was supported by the Platform Construction Fund of the 7T Magnetic Resonance Imaging Translational Medicine Center of Southwest Hospital (No. 524Z2Q31) and the Special Project for Enhancing Technological Innovation Capability of Army Medical University (No. 2023XQN31).

Author Contribution

Conceptualization, Z.Z. (Zhen) and S.Z.; Data curation, D.Y.; Formal analysis, Y.H.; Funding acquisition, W.C.; Investigation, L.Y., Z.S., and M.L.; Methodology, Y.H. and P.H.; Supervision, C.L. and W.C.; Writing – original draft, Z.Z. and S.Z.; Writing – review & editing, Y.C.H., Z.Z. (Zuo), P.H., C.L., and W.C. Z.Z. (Zhen), S.Z., and L.Y. contributed equally to this work. All authors read and approved the final manuscript.

Data Availability

The data that support the findings of this study are available from the corresponding author upon reasonable request.

References

1. Saunders NR, et al. The choroid plexus: a missing link in our understanding of brain development and function. Physiol Rev. 2023;103(1):919–56.
2. Lai G, et al. The aging choroid plexus and its relationship with gut dysbiosis and Klotho decline: possible intervention strategies. Geroscience. 2025;47(6):6869–83.
3. Jang A, Lehtinen MK. Experimental approaches for manipulating choroid plexus epithelial cells. Fluids Barriers CNS. 2022;19(1):36.
4. Lin M, et al. Association Between Choroid Plexus Morphological Alterations, Alzheimer Pathologies, and Cognitive Impairment: A Longitudinal Study. Neurology. 2025;105(12):e213953.
5. Courtney Y, Hochstetler A, Lehtinen MK. Choroid Plexus Pathophysiology Annu Rev Pathol. 2025;20(1):193–220.
6. Li Y, et al. Choroid Plexus Enlargement Exacerbates White Matter Hyperintensity Growth through Glymphatic Impairment. Ann Neurol. 2023;94(1):182–95.
7. Čarna M, et al. Pathogenesis of Alzheimer's disease: Involvement of the choroid plexus. Alzheimers Dement. 2023;19(8):3537–54.
8. Diez-Cirarda M, et al. Choroid plexus volume is enlarged in long COVID and associated with cognitive and brain changes. Mol Psychiatry. 2025;30(7):2821–30.
9. Sun Z, et al. Age-related Vascular Alterations in the Choroid Plexus: Novel Insights from Pathophysiology and Imaging Studies. Aging Dis; 2025.
10. Li K, et al. Characterizing choroid plexus cyst burden across the Alzheimer's disease continuum. Fluids Barriers CNS. 2025;22(1):122.
11. Zhen Z, et al. Choroid plexus cysts on 7T MRI: Relationship to aging and neurodegenerative diseases. Alzheimers Dement. 2025;21(2):e14484.
12. Sun Z, et al. Choroid plexus aging: structural and vascular insights from the HCP-aging dataset. Fluids and Barriers of the CNS; 2024. p. 21.
13. Stanishevskiy A et al. Symptomatic intraventricular choroid plexus cysts. Illustrative case and systematic review. Neurosurg Rev, 2023. 46.

14. Ki Seong E. Spontaneous bilateral disappearance of choroid plexus cysts in the trigone of the lateral ventricles: a case report. Turkish Neurosurgery; 2024.
15. Shirazinejad S, Moradi H, Khanjani S. Natural history and prognostic significance of fetal choroid plexus cysts: a systematic review. BMC Pregnancy and Childbirth; 2026.
16. Gong Z, et al. Age-related differences in choroid plexus structural integrity are associated with changes in cognition. Fluids and Barriers of the CNS; 2025.
17. Murakami R, Ueno M. Morphological and Molecular Characteristics of Choroid Plexus Epithelium in Aged Brains. Int J Mol Sci. 2026;27:2505.
18. Scarpetta V, et al. Choroid plexus: Insights from distinct epithelial cellular components. Curr Opin Neurobiol. 2025;93:103028.
19. *Age-related Vascular Alterations in the Choroid Plexus: Novel Insights from Pathophysiology and Imaging Studies*. aging and disease, 2025.
20. Chen L et al. Choroid plexus cyst burden is associated with glymphatic dysfunction and cognitive impairment in hepatic encephalopathy. Hepatol Commun, 2026. 10.
21. Liu L, et al. Choroid plexus enlargement contributes to motor severity via regional glymphatic dysfunction in Parkinson's disease. NPJ Parkinsons Dis. 2025;11(1):134.
22. Sun Z, et al. Advanced MRI of the choroid plexus: Applications in aging and dementia. Journal of Cerebral Blood Flow & Metabolism; 2026.

Figures

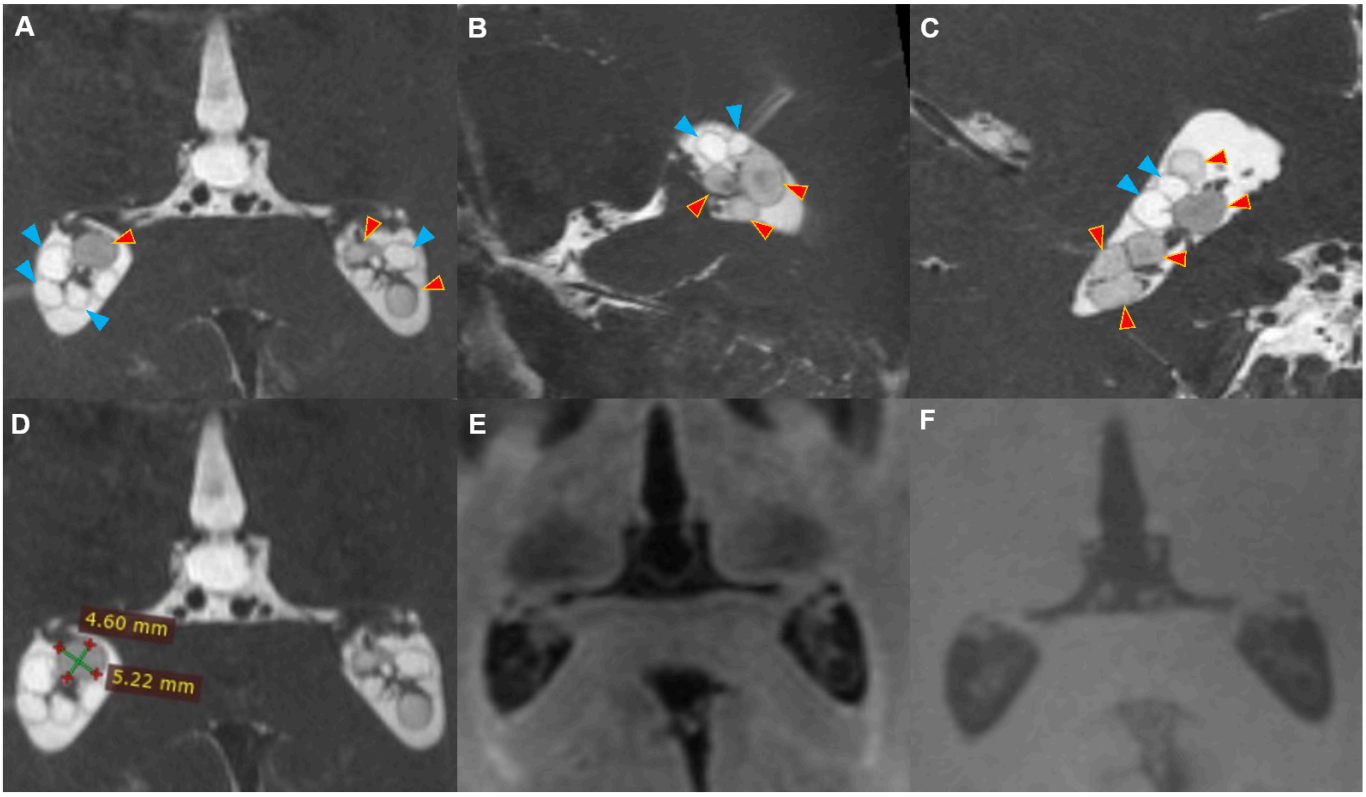


Figure 1

Multiplanar MRI characteristics and quantitative assessment of choroid plexus cysts (CPCs). (A–C) Representative T2-weighted SPACE images showing CPCs in the axial (A), sagittal (B), and coronal (C) planes. Two imaging phenotypes were identified according to cyst signal intensity: hypointense CPCs (red arrowheads), with signal intensity lower than that of the surrounding CSF, and CSF-like CPCs (blue arrowheads), with signal intensity similar to that of CSF. (D) Illustration of CPC morphometric assessment, with three orthogonal diameters measured for volume estimation. (E) Corresponding T2-FLAIR image. (F) Due to their thin walls and T1-signal intensity similar to that of CSF, CPCs are often not discernible on conventional T1-weighted images.

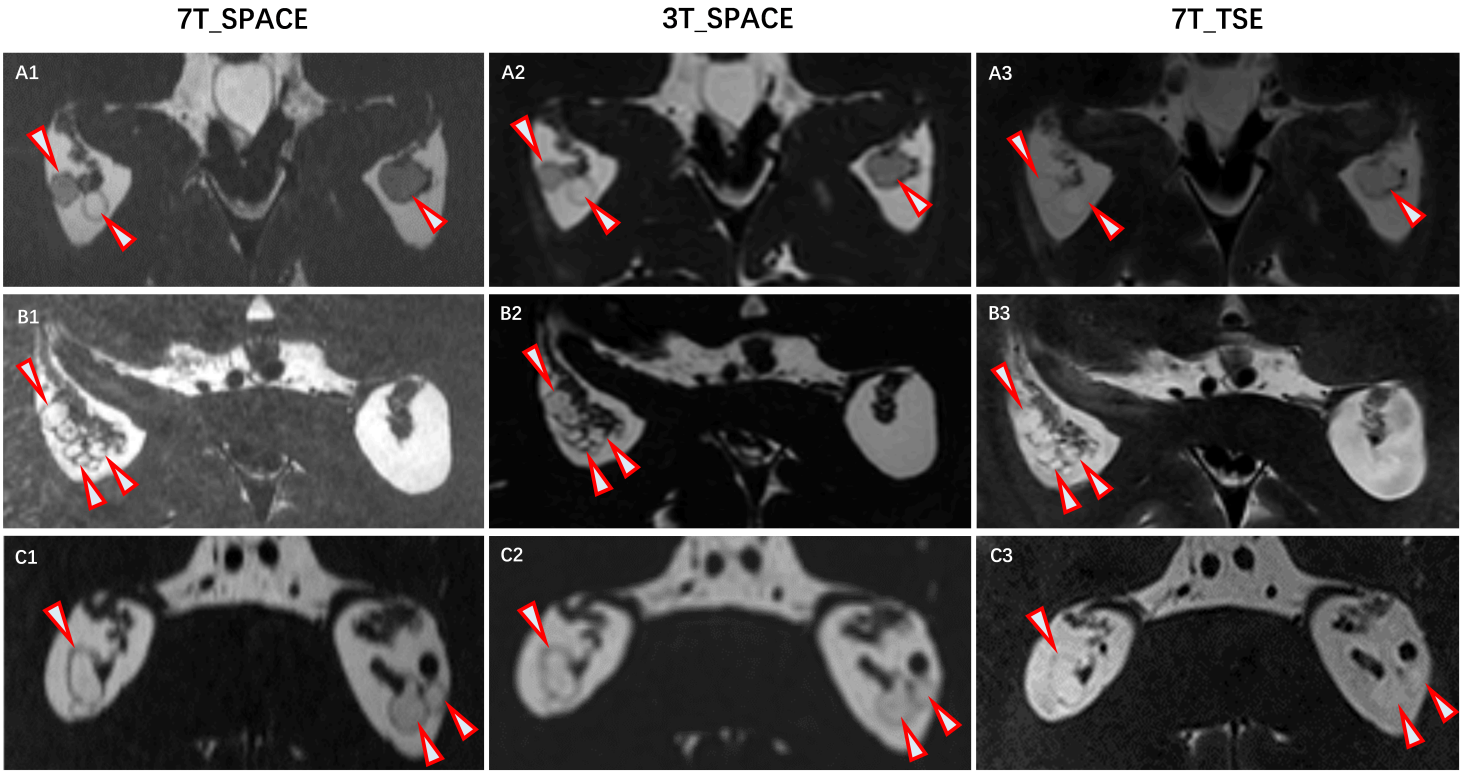


Figure 2

Comparative visualization of choroid plexus cysts (CPCs) across7T and 3T MRI protocols. Representative images of the same anatomical regions acquired using 7T SPACE (A1, B1, C1), 3T SPACE (A2, B2, C2), and 7T TSE (A3, B3, C3) are shown. Both 7T SPACE and 3T SPACE provide clear delineation of CPCs, with relatively sharp and continuous cyst walls and well-defined internal septations, allowing detailed assessment of cyst morphology and size. In contrast, CPC walls are less completely visualized on 7T TSE images, with less distinct margins and mild imaging artifacts. Hypointense CPCs show similar signal characteristics on 7T and 3T SPACE images, whereas these features are less conspicuous on 7T TSE images. Red arrowheads indicate corresponding CPCs across the three imaging protocols.

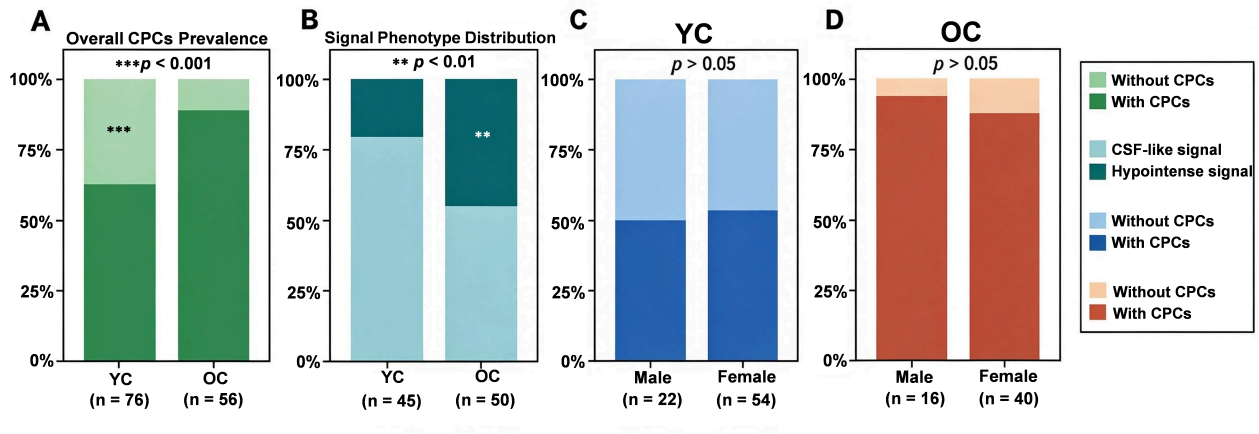


Figure 3

Distribution of choroid plexus cysts (CPCs) across age cohorts and by sex.

(A) Overall prevalence of CPCs in the younger cohort (YC) and older cohort (OC). Green and light-green segments indicate participants with and without CPCs, respectively. (B) Distribution of CSF-like and hypointense CPC phenotypes in the YC and OC. (C, D) Sex-based comparisons of CPC prevalence within the YC and OC, respectively. Orange and blue segments indicate participants with and without CPCs, respectively. Statistical comparisons were performed using Fisher's exact test where applicable (***P < 0.001). Sample sizes (n) are shown in parentheses.

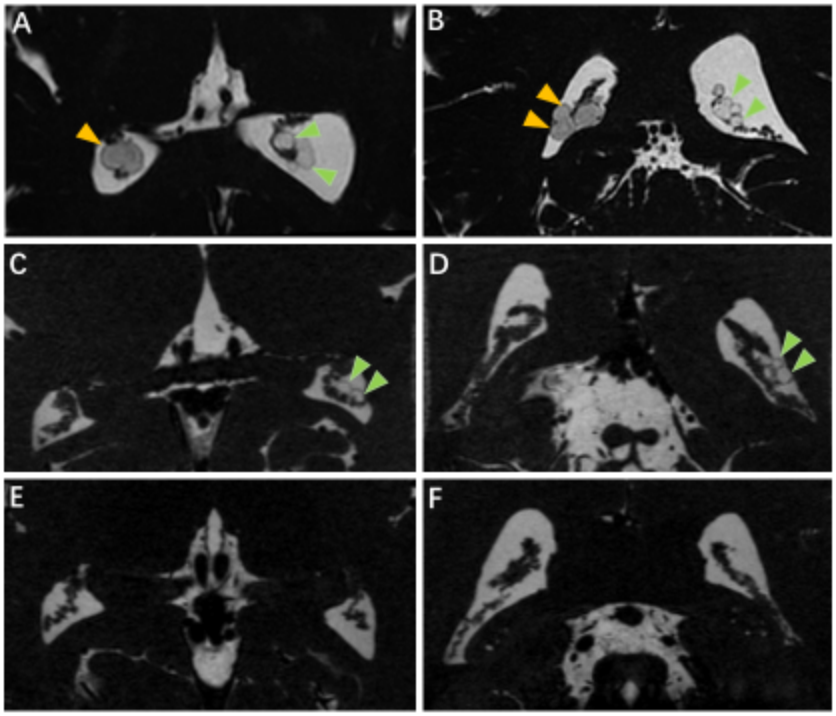


Figure 4

Representative MRI phenotypes of choroid plexus cysts (CPCs) on axial and coronal T2-weighted images.

(A, B) Representative images from an older participant showing coexisting hypointense CPCs (orange arrowheads) and CSF-like CPCs (green arrowheads). (C, D) Representative images from a younger participant showing exclusively CSF-like CPCs (green arrowheads). (E, F) Representative images from a younger participant without visible CPCs, demonstrating the typical appearance of the choroid plexus within the lateral ventricles.

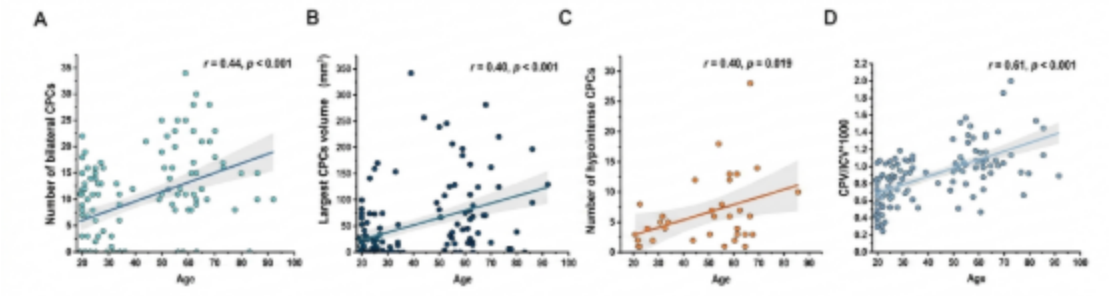


Figure 5

Associations between age and choroid plexus morphometric characteristics. Scatter plots with fitted regression lines and 95% confidence intervals illustrate the relationships between age and (A) total CPC count, (B) bilateral largest-CPC volume, (C) number of hypointense CPCs, and (D) normalized choroid plexus volume (CPV) across the study population. Bilateral largest-CPC volume was defined as the sum of the volumes of the largest CPC identified in each hemisphere. Normalized CPV was calculated as CPV/TIV × 1,000. CPC, choroid plexus cyst; CPV, choroid plexus volume; TIV, total intracranial volume.

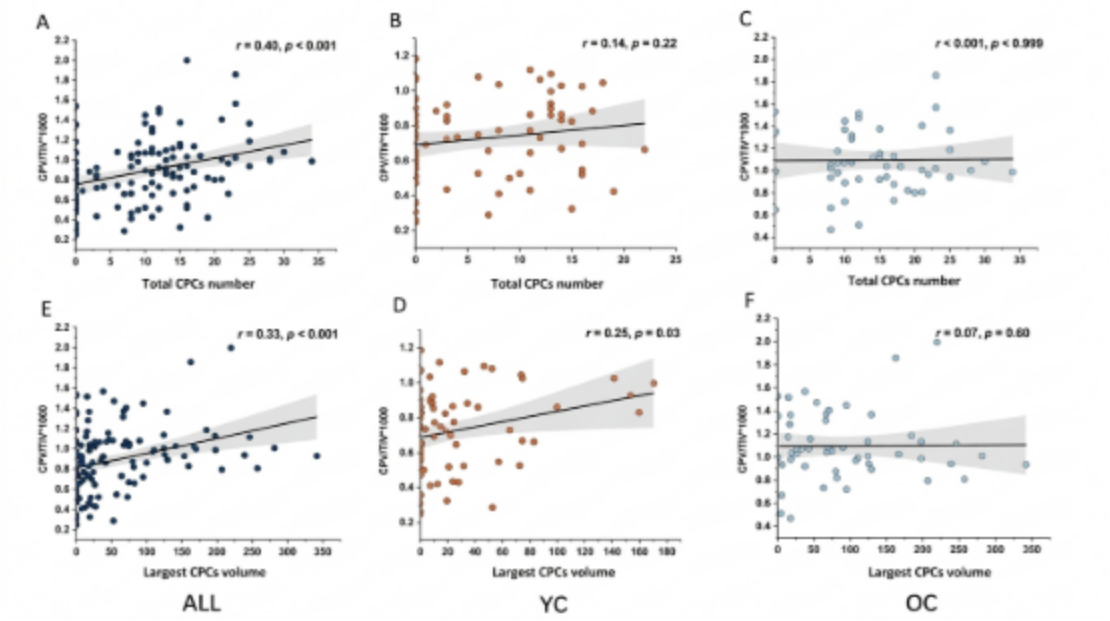


Figure 6

Associations between cystic burden and normalized choroid plexus volume (CPV) across groups. Significant positive associations were observed in the overall population, and normalized CPV was also significantly associated with bilateral largest-CPC volume in the YC. In contrast, no significant associations were observed between normalized CPV and either CPC measure in the OC. ALL, entire study population; YC, younger cohort; OC, older cohort; CPC, choroid plexus cyst; CPV, choroid plexus volume; TIV, total intracranial volume.